Lawrence Berkeley National Laboratory
LBL Publications

Title

Influence of Wind Direction on Thermodynamic Properties and Arctic Mixed-Phase Clouds in Autumn at Utqiaġvik, Alaska

Permalink

https://escholarship.org/uc/item/8hk91057

Journal

Journal of Geophysical Research: Atmospheres, 123(17)

ISSN

2169-897X

Authors

Qiu, Shaoyue
Xi, Baike
Dong, Xiquan

Publication Date

2018-09-16

DOI

10.1029/2018jd028631

Peer reviewed

eScholarship.org Powered by the California Digital Library
University of California

Influence of Wind Direction on Thermodynamic Properties and Arctic Mixed-Phase Clouds in Autumn at Utqiaġvik, Alaska

Shaoyue Qiu[1], Baike Xi[1], and Xiquan Dong[1]

1 Department of Hydrology and Atmospheric Sciences, University of Arizona, Tucson, AZ, USA

Correspondence to: B. Xi, baike@email.arizona.edu

Abstract

Seven years of autumnal ground-based observations (September–November 2002–2008) at the U.S. Department of Energy Atmospheric Radiation Measurement North Slope of Alaska site have been analyzed for addressing the occurrence frequency and macrophysical and microphysical properties of Arctic mixed-phase clouds (AMC), as well as the relationship between environmental parameters and AMC properties. In September and October, AMC occurrence frequency is 20–30% lower during a southerly wind when compared to the other wind directions; in November, the variation of AMC occurrence frequency with wind direction is small. The mean liquid water path in November is about half of that in October and September. When the surface is snow free, temperature (T) and specific humidity (q) profiles during a northerly wind are warmer and moister than those for the southerly wind. Northerly wind profiles have a higher relative humidity to ice (RH_i) and lower atmosphere stability. Furthermore, the AMC occurrence frequency has a positive relationship with RH_i and a negative relationship with stability. These two points may explain the lower AMC occurrence frequency during a southerly wind. During a northerly wind, AMCs have larger radar reflectivity, wider spectrum width, and larger Doppler velocity signatures. The stronger precipitation for AMC during a northerly wind is possibly due to the cleaner air masses from the ocean (north). With the same amount of q, the radar spectrum width has a higher frequency in the larger bins during a northerly wind. Both T, q, and radar reflectivity, radar spectrum width profiles show evidence of deposition in the sub-cloud layer in September and October.

1 Introduction

Model simulations and observations show that the Arctic is one of the most sensitive regions with respect to global climate change (Cohen et al., 2014; Holland & Bitz, 2003; Johannessen et al., 2004; Najafi et al., 2015; Schuur et al., 2015; Serreze et al., 2009). Clouds, especially liquid-containing clouds, are the main modulator of surface and top of atmosphere radiation. Their net radiative forcing over the Arctic is ~20 to 30 W/m^2 in winter season and ~ −30 to −20 W/m^2 in summer season (Dong et al., 2010; Shupe & Intrieri, 2004). Furthermore, clouds remain one of the largest uncertainties in our understanding of the climate, climate modeling, and prediction. Recent studies show that due to the underestimation of the supercooled liquid fraction in mixed-phase clouds in climate models, the equilibrium climate sensitivity could change up to 1.3 °C under the doubling of atmosphere CO_2

scenario (Tan et al., 2016). The underestimation of liquid cloud fraction also contributes to a 2–3 °C cold bias for surface temperature over the Arctic in summer (Kay et al., 2016).

Mixed-phase clouds are the dominant low-level cloud type over the Arctic with an annual occurrence frequency of ~45% (Qiu et al., 2015; Shupe, 2011). Furthermore, different from mixed-phase clouds at lower latitudes, Arctic mixed-phase clouds (AMCs) often occur as a stratiform type and can persist for hours to days, and sometimes even weeks (de Boer et al., 2009; Dong & Mace, 2003; Qiu et al., 2015; Shupe et al., 2006, 2008; Verlinde et al., 2007; Wang et al., 2004). Because of their high frequency of occurrence and significant influence on the surface radiation budget, AMCs and their maintenance mechanisms have been studied substantially over the past several decades, and progresses have been achieved toward our understanding of the AMCs. For example, the liquid layer at cloud top structure enhances the cloud top radiative cooling, which generates turbulence in the cloud and forces direct condensation (Pinto, 1998; Solomon et al., 2011; Zuidema et al., 2005). The persistent temperature and moisture inversions above the mixed-phase cloud provide moisture through entrainment and compensate the moisture loss due to precipitation and sedimentation (Qiu et al., 2015; Sedlar et al., 2012; Sedlar & Tjernström, 2009; Solomon et al., 2011). The lack of aerosols and ice nuclei over the Arctic also impedes the ice formation process in mixed-phase clouds and therefore slows down the transformation from a mixed-phase cloud to an ice cloud (Jiang et al., 2001).

In general, AMCs have complex and close interactions with the surrounding environment. Through these interactions, AMCs can maintain their self-sustaining mechanisms and thus have a longer lifetime than mixed-phase clouds in the midlatitudes (Morrison et al., 2012). Furthermore, the dissipation processes that destroy midlatitude stratiform clouds, such as precipitation, convective heating from the surface, and absorption of solar radiation, are often either nonexistent and/or are relative weak in the Arctic (Dong & Mace, 2003). Despite these progresses in understanding AMCs, their sustaining mechanisms are still poorly understood and are not well simulated in models (Klein et al., 2009; Morrison et al., 2009; Xie et al., 2013). Therefore, it is necessary to investigate AMC-sustaining mechanisms using long-term ground-based observations. For instance, to what extent do AMCs associate with atmospheric thermodynamic variables and different air masses transported from the ocean and land?

In autumn (September to November), the Arctic surface transitions from snow free to snow/ice covered at the Atmospheric Radiation Measurement North Slope of Alaska Utqiaġvik site. Thus, the site is an ideal location for studying how surface conditions influence atmospheric thermodynamic properties and thereby influence cloud formation and properties (Curry et al., 1996). Furthermore, both AMC occurrence frequency and lifetime are highest and longest in autumn according to ground-based observations (Shupe,

2011; Shupe et al., 2011). Qiu et al. (2015) found that the AMC occurrence frequency increases with stronger moisture inversions in winter, which indicates that moisture inversions may serve as a moisture source for the AMC. However, despite the high AMC occurrence frequency in autumn, humidity inversions occur less frequently and have the weakest inversion intensity (Devasthaleet al., 2011; Nygård et al., 2013; Qiu et al., 2015). Therefore, it is imperative to investigate the interactions between AMC and thermodynamic variables other than moisture during this transition season. Due to the coastal location of the Utqiaġvik site, marine air masses are transported by northerly winds, while more continental air masses are transported by southerly winds. Therefore, this site provides a unique opportunity to study the influence of both surface conditions and different air masses on thermodynamic variables and on AMC properties.

2 Data and Methodology

In this study, autumnal thermodynamic profiles, as well as mixed-phase cloud properties at the Atmospheric Radiation Measurement (ARM) North Slope of Alaska (NSA) site, have been analyzed using a combination of cloud radar, lidar, microwave radiometer, and sounding measurements (for detailed site information refer to Stokes and Schwartz, 1994, and Stamnes et al., 1999). Cloud top height is derived from the millimeter wavelength cloud radar (Moran et al., 1998), and cloud base heights are derived from the micropulse lidar (MPL; Campbell et al., 1998, 2002) and ceilometer measurements (Flynn, 2004; Morris, 2012). Since the MPL has shorter wavelength and higher emitted power, as well as a less strict definition of clouds in their cloud base (Z_b) retrieval algorithm, the MPL is more sensitive to optically thin ice clouds than the ceilometer (Campbell et al., 1998, 2002; Clothiaux et al., 1998; Turner, 1996). In this study, ceilometer and MPL Z_b are from the Active Remote Sensing of Clouds data (Clothiaux et al., 2000), where the $Z_{b,ceil}$ is calculated by a built-in algorithm developed by the manufacturer (Flynn, 2004), and the $Z_{b,MPL}$ algorithm is based on Campbell et al. (1998) and Clothiaux et al. (1998).

$Z_{b,ceil}$ is frequently used as the liquid layer boundary located at the upper part of the AMC. That is, the strong backscatter data from the ceilometer and MPL, combined with the small depolarization ratio from the MPL, indicate the existence of liquid phase droplets in this layer. Qiu et al. (2015) found that the MPL-defined Z_b is usually several hundred meters to 1 km lower than the ceilometer Z_b. In the region between $Z_{b,MPL}$ and $Z_{b,ceil}$, the backscatter data range from 8 to 30 $\times 10^{-6}$/m·sr, the depolarization data fall between a range of 0.1–0.5, and the Doppler velocity is often less than 1 m/s (Qiu et al., 2015). Therefore, this layer between the two cloud bases should be defined as ice cloud, in which $Z_{b,MPL}$ defines the lower boundary of the ice layer. Below $Z_{b,MPL}$, both ceilometer and MPL backscatter are less than 2 $\times 10^{-6}$/m·sr. Therefore, it is defined as the ice virga layer. The large particle size and small number concentration of ice virga below $Z_{b,MPL}$ can be detected by radar, with reflectivity ranging between −40 and 0 dBZ. But it cannot be

distinguished by either the ceilometer or the MPL measurements (Qiu et al., 2015). In this study, we will continue use the $Z_{b,ceil}$ and $Z_{b,MPL}$ to define the vertical structure of an AMC, and different physical processes in the different layers of an AMC will be further investigated in section 3.3.

Cloud liquid water path (LWP) is retrieved from the microwave radiometer (MWR) measured brightness temperatures (Liljegren et al., 2001). Atmospheric thermodynamic variables are from the ARM-merged sounding product, which combines radiosonde observations, surface meteorological observations, and output from the European Center for Medium-Range Weather Forecast model (Troyan, 2012). All of the instruments and data used in this study (millimeter wavelength cloud radar, MPL, ceilometer, MWR, merged sounding data, etc.) have been widely used to study cloud properties and atmospheric conditions over the Arctic (Dong & Mace, 2003; Intrieri et al., 2002; Sedlar et al., 2012; Sedlar & Shupe, 2014; Sotiropoulou et al., 2014; Shupe et al., 2006, 2008, 2011; Wang et al., 2004; Zuidema et al., 2005; Wesslén et al., 2014). This investigation will use the data sets during the period from January 2002 to December 2008 given the overlapping availability of all data sets.

Since this study primarily focuses on investigating the impacts of different surface conditions, air masses, and atmospheric thermal conditions on AMC properties, we have selected low-level AMCs with a cloud top below 3 km. The classification of AMCs follows the method in Shupe (2007), which used an integrated analysis of MPL depolarization data (Intrieri et al., 2002; Sassen, 1991), lidar backscatter data, and MWR-retrieved cloud LWP. In this study, a mixed-phase cloud is defined as the coexistence of liquid cloud droplets and ice particles in the same cloud layer. In addition, this study does not distinguish between single layer or multilayer clouds, such that if a mixed-phase cloud exists at a time step, this time step is classified as mixed-phase cloudy condition.

The surface wind is classified into four 90° sectors (for example, a northerly wind is 0° ± 45°). Advection of specific air masses is assessed based upon the mean wind direction from the surface to 950 hPa (~500 m). The relative frequency distribution (RFD) of the wind direction data is examined, and the results demonstrate that wind direction is nearly invariant with height from the surface to 3 km in autumn at the ARM NSA site (not shown). That is, results and conclusions of this study are nearly the same regardless of level at which the wind direction is analyzed (e.g., at the surface, 500-m level, or 1,500-m level).

We also examine the uncertainties of the wind direction data and thermodynamic parameters in the merged sounding product by repeating results with merged sounding data near the radiosonde launch time ±30 min only. The RFD of wind directions over height and the RFD of thermodynamic profiles during different wind directions do not change between these two sample populations (not shown). Therefore, we can conclude that the wind

direction and the thermodynamic parameters of the merged sounding product can represent the wind properties and the AMC thermodynamic properties between different wind directions at the Utqiaġvik site.

3 Results

3.1 Cloud Properties

As shown in Figures 1a–1c, an easterly wind is observed to be the most common wind direction at Utqiaġvik with a frequency of 50–60% from September to November; the other three wind directions occur at 10–20%. The monthly mean low-level AMC occurrence frequencies are 42.1%, 49.9%, and 33.8%, respectively, from September to November. Moreover, the AMC occurrence frequencies in September and October vary from ~30% when there is a southerly wind to ~40–60% for the other three wind directions, indicating that the air mass or thermodynamic variables that are being advected from the south are significantly different from other directions and may not be favorable for AMCs formation and/or sustainment. Due to the geographic location of the NSA site, oceanic air masses can come from all directions except from the south. In November, as both land and ocean are covered by snow/ice, the AMC occurrence frequencies have much smaller variations between the four wind directions.

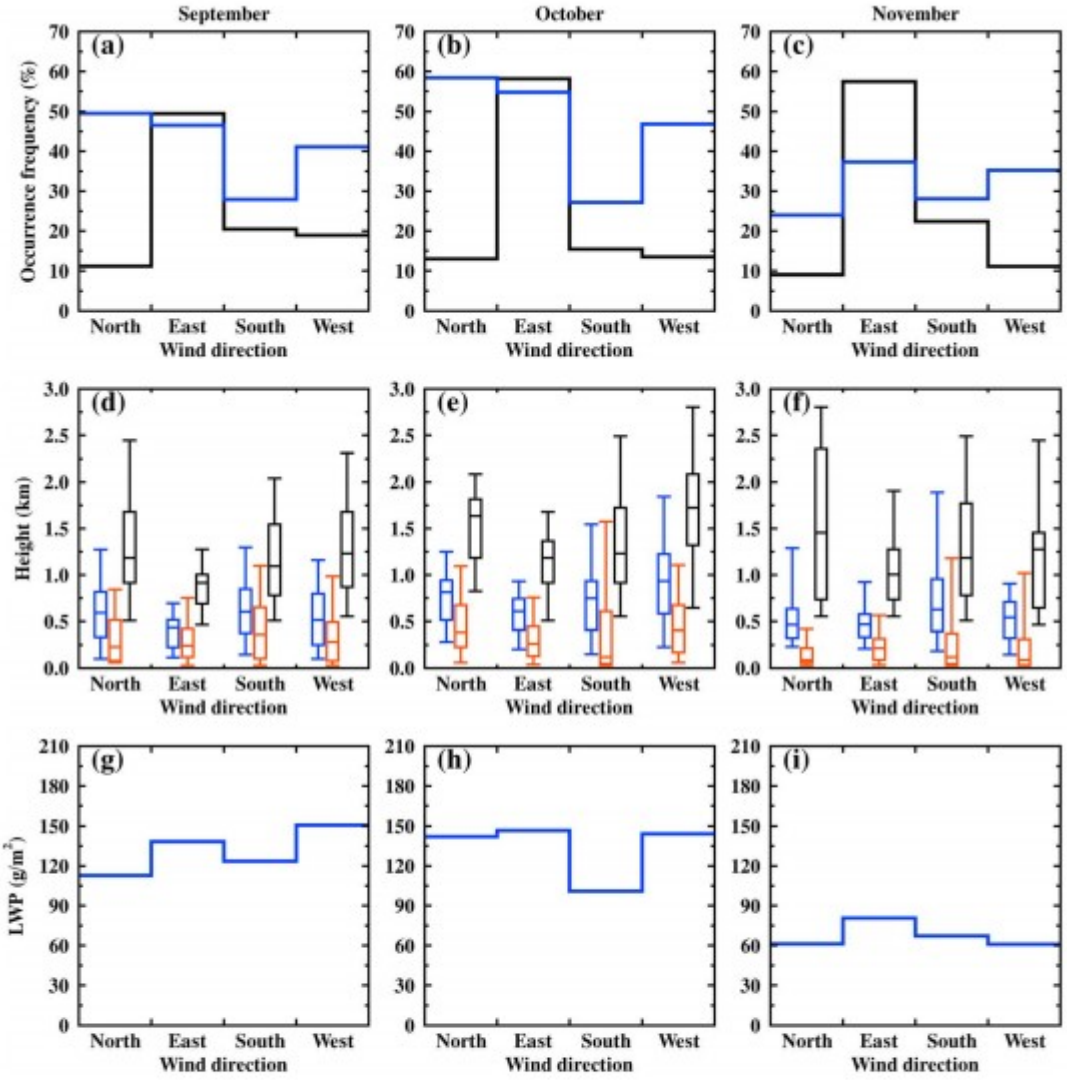

Figure 1. Occurrence frequencies of low-level Arctic mixed-phase clouds (AMC top height ≤ 3 km), wind, cloud base/cloud top heights, and LWPs during different wind directions at the Atmospheric Radiation Measurement North Slope of Alaska (ARM NSA) site from September to November during the period 2002–2008. (a–c) The occurrence frequencies of wind (black lines) and AMCs (blue). (d–f) The box and whisker plots of AMC cloud top (black lines, derived from ARM cloud radar), ceilometer-derived cloud base (blue lines), and MPL-derived cloud base (red lines). The whisker diagram includes the median (middle bar), 25th and 75th percentiles (ends of boxes) and 5th and 95th percentiles (lower and upper bar). (g–i) AMC mean LWPs for different wind directions.

The median cloud top (black lines) and $Z_{b,ceil}$ heights (blue lines) in September are 1.01 and 0.47 km, respectively. The median values in November are very close to those in September, but the median cloud top and cloud base heights in October are about 200–300 m higher than those in September and November. The mean cloud thickness (the difference between radar cloud top and $Z_{b,ceil}$) is similar between the three months, with mean values of 0.54, 0.60, and 0.57 km from September to November, respectively. The MPL-derived cloud bases (red lines) from the three months are close to the ground, ranging from 0.21 km in November to 0.29 km in

October. The ice layer thicknesses, which is defined as the difference between ceilometer and MPL cloud bases, as discussed in the previous section, are 0.22, 0.41, and 0.27 km from September to November, respectively. There are relatively large variations of cloud top heights for different wind directions, where the cloud top heights during the northerly and westerly winds are generally higher than those during the easterly and southerly winds.

AMC LWPs exhibit similar monthly means in September (135.2 g/m^2) and October (141.5 g/m^2) but are significantly lower in November (74.8 g/m^2). In September, the AMC LWP during a southerly wind is slightly larger than that of the northerly wind. However, in October the AMC LWPs are much smaller for southerly winds compared to the other wind directions. This is likely due to the accumulation of snow on the ground in October, which would prevent the interaction of heat and moisture between the land and atmosphere, reduce the specific humidity, and further decease cloud LWP (Lin et al., 2003; Wall et al., 2017). A positive relationship is found between the atmospheric specific humidity and cloud LWP in this study (not shown). Influence of surface condition on the thermodynamic variables in different months will be discussed in the next section. In November, when both the ocean and land are ice/snow covered, the AMC LWPs are much lower and have a smaller variation between different wind directions.

Considering the distinguishable AMC characteristics in autumn with wind directions, in the next section, we attempt to isolate four thermodynamic properties responsible for controlling AMC properties and associate them with different wind directions.

3.2 Thermodynamic Profiles and Their Relationship With Mixed-Phase Clouds

The profiles of atmospheric temperature, specific humidity, relative humidity, and stability (defined by equivalent potential temperature gradient) during northerly and southerly winds are plotted in Figures 2-4, for September, October, and November, respectively. Based on the geographic location of the Utqiaġvik site, easterly/westerly winds occur under the influence from either the ocean (e.g., NE/NW wind) or the land (e.g., SE/SW wind). Additionally, both the easterly and westerly wind thermodynamic profiles are similar to those during the northerly wind. Therefore, only northerly and southerly wind profiles are shown here to represent the contrast between ocean and land air masses. To investigate the interactions between thermodynamic properties and the cloud layer, the profiles are normalized by cloud base and cloud top heights. As discussed before, both ceilometer and MPL-derived cloud bases are used to better characterize AMC vertical structure.

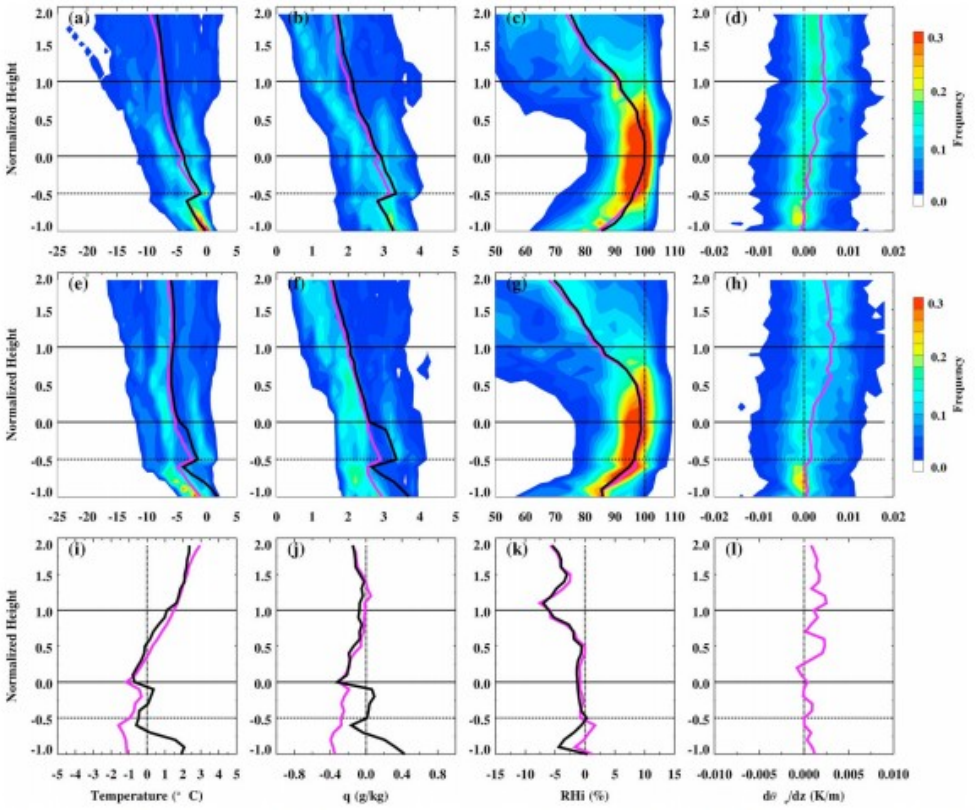

Figure 2. The relative frequency distribution contours of (a, e) temperature (°C), (b, f) specific humidity (g/kg), (c, g) RH with respect to ice (%), and (d, h) equivalent potential temperature gradient (K/m) for AMCs in September at the ARM NSA site during the period 2002–2008. The top panels (a–d) are profiles during the northerly wind, and the middle panels (e–h) are during the southerly wind. The 100% RH value and zero value for $d\,\theta_e/dz$ are highlighted with dots in (c), (g), (d), and (h). The black lines are median profiles for all cloud types (as reference), and the magenta lines are the median profiles for AMCs. The bottom panels (i–l) are the difference in median values (southerly wind minus northerly wind) for all cloud types (black lines) and AMCs (magenta lines).The normalized height is defined as follows: $Z_n = -1$ is the radar first range gate (105 m above ground level), $Z_n = -0.5$ is the MPL cloud base (dash lines), $Z_n = 0$ is the ceilometer cloud base (black solid lines), $Z_n = 1$ is the radar cloud top (black solid lines), and $Z_n = 2$ is one cloud thickness (the difference between cloud top and ceilometer derived cloud base) above the cloud top.

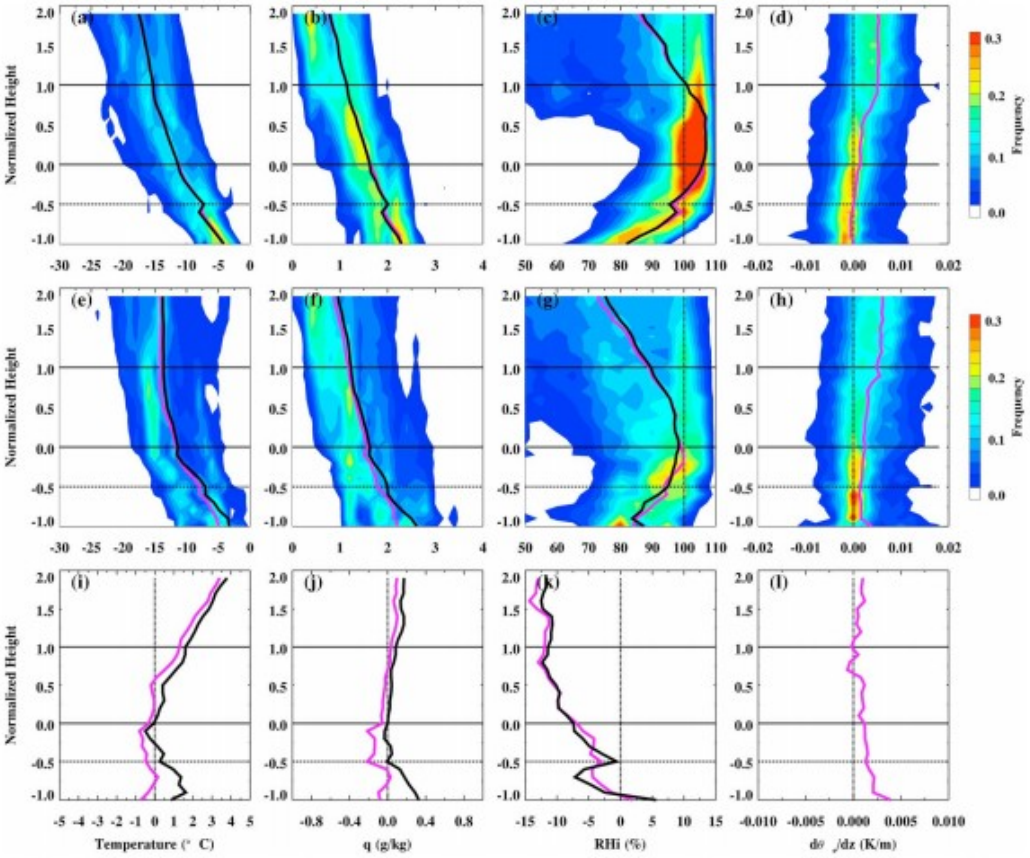

Figure 3. Same as Figure 2, but for October.

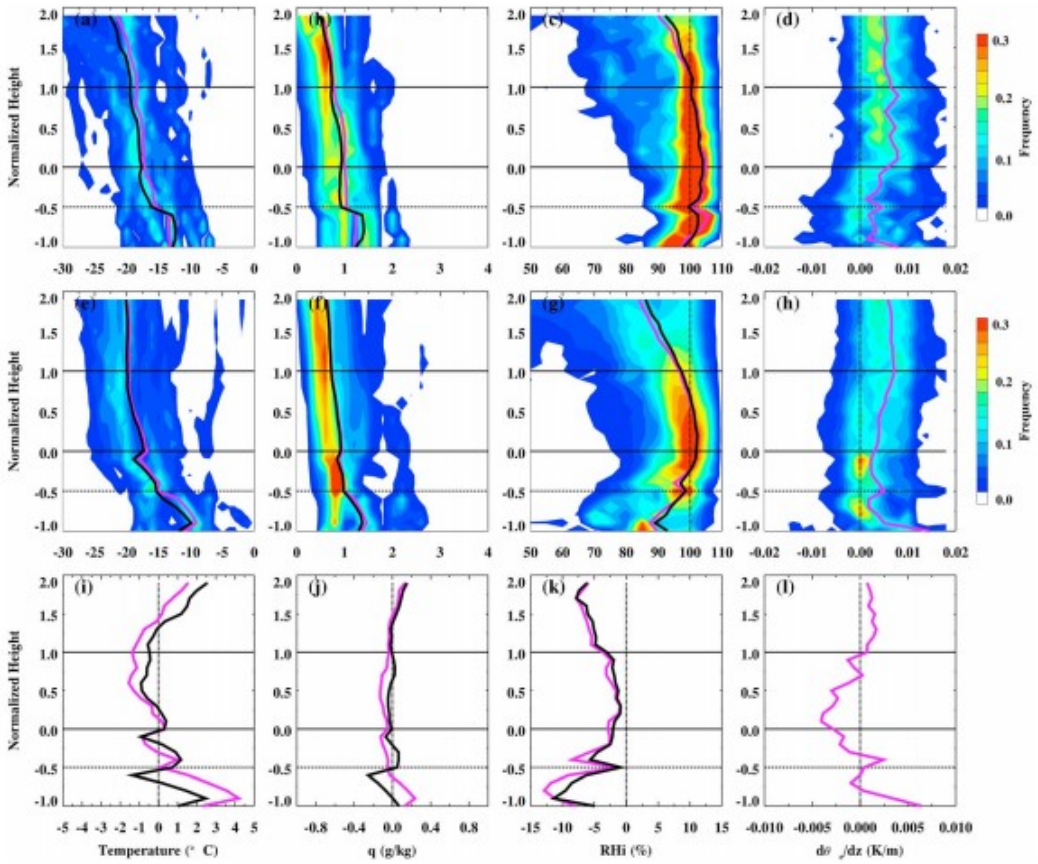

Figure 4. Same as Figure 2, but for November.

Figure 2 shows that strong temperature and specific humidity inversions exist below $Z_{b,MPL}$ in an AMC layer (dashed line, $Z_n = -0.5$), and weak inversions also exist below $Z_{b,ceil}$ ($Z_n = 0.0$). This result is different than the results determined over northern Alaska, where temperature and moisture inversions occur more often above the AMC rather than below it (Curry et al., 1996; Qiu et al., 2015; Sedlar et al., 2012). It is because results shown here are the median values and relative frequency distributions for all sounding profiles; if inversions exhibited at different levels relative to the cloud, they will be averaged out. Statistics of the inversions on a profile-by-profile basis would show a different result, as was done in Qiu et al. (2015). The specific humidity inversions below the cloud base could be due to the deposition of water vapor on the falling ice crystals in the sub-cloud layer, which would cause the specific humidity to decrease. Different processes in different parts of the AMC will be discussed in detail in section 3.3.

During a southerly wind, the mixed-phase cloud conditions are colder and drier than all low-cloud conditions, especially below $Z_{b,MPL}$ (magenta and black lines in Figures 2e and 2f). Comparing the northerly and southerly wind profiles, the maximum frequency of temperature is ~0 °C at the surface during a northerly wind and ~ −2 °C during a southerly wind. The difference in median value (southerly wind minus northerly wind) is 0.25–1 °C colder

below the cloud, while it is up to 3 °C warmer inside and above the cloud (Figure 2i). Meanwhile, the southerly wind is drier than the northerly wind profile in both the maximum frequency and the median value of specific humidity. This result agrees with our assumption that air coming from the ocean should be moister than from the land. Furthermore, the northerly and southerly wind temperature and specific humidity profiles are significantly different from each other at 99.9% confidence level.

The relative humidity with respect to ice (RH_i) median values increase from ~85% (82%) at the surface to a maximum of ~100% around the $Z_{b,ceil}$ and then deceases to ~90% (84%) at the cloud top for the northerly (southerly) wind conditions. On average, the median RH_i values are slightly higher for the northerly wind conditions, especially within the cloud layer (Figure 2k). This vertical profile of the RH_i for AMC is similar to the RFD of RH_i profiles for the coupled Arctic stratocumulus cloud in Sotiropoulou et al. (2014).

Figures 2d and 2h illustrate the equivalent potential temperature (θ_e) gradient profiles. A negative or zero gradient of θ_e indicates that the layer is unstable or well mixed, while a positive gradient represents a more stable atmosphere. One benefit of using θ_e instead of potential temperature (θ) is to include the latent heat effect on the lifted parcel. This extra heating may cause a saturated parcel to be unstable even if θ increases with height. In September, AMCs are usually coupled to the surface, with the median $d\,\theta_e/dz$ value around zero below $Z_{b,MPL}$. Above $Z_{b,MPL}$, $d\,\theta_e/dz$ gradients become positive and they increase until the cloud top. There are minor differences in the atmospheric stability profiles between northerly and southerly winds in September.

The easterly and westerly thermodynamic profiles are similar to that during a northerly wind (not shown). AMCs are usually coupled to the surface during easterly and westerly winds. During an easterly wind, AMCs are slightly warmer compared with the other three wind directions, especially at cloud top (~2–5 °C warmer), so that the relative humidity to ice is much lower at the cloud top (~75%) during an easterly wind. This instant drying of the atmosphere at a higher level during an easterly wind is also seen in the RH_i profile with standard height (not shown), which may explain the lower cloud top heights for AMCs during an easterly wind, as shown in Figure 1d.

In October (Figure 3), as the Beaufort Sea is usually relatively open, while the northern Alaska starts to be covered by snow, the differences of atmospheric temperature and specific humidity between the northerly and southerly winds are larger compared to those in September. When the wind originates from the ocean (north), the air mass is more homogeneous and the RFDs of temperature and specific humidity are narrower than those from over land (south), as shown in Figures 3a, 3b, 3e, and 3f. Similar as in September, the northerly wind profiles have higher frequencies in warmer temperature and larger specific humidity. Temperature and specific humidity inversions occur below the $Z_{b,MPL}$.

The atmosphere is more saturated during the northerly wind. As demonstrated in Figure 3c, both the maximum distribution and the median value of RH_i are greater than 100% in the cloud layer during the northerly wind. During the southerly wind shown in Figure 3g, RH_i is close to saturation in the ice layer, with a range of RH_i values from 92 to 98%. Furthermore, the maximum frequency of $d\,\theta_e/dz$ below $Z_{b,ceil}$ is less than zero with its median value close to zero during the northerly wind, so that AMCs are likely coupled to the surface (Figure 3d). When the wind is coming from the south, the maximum frequency of $d\,\theta_e/dz$ is close to zero and the median value is larger than zero, and it increases toward the surface so that the clouds are likely decoupled from the surface (Figure 3h).

These differences in the thermodynamic profiles between the southerly and northerly wind could partially explain the 20–30% lower occurrence frequency of AMCs during the southerly wind compared with the other wind directions at the ARM NSA site. The more stable atmosphere below the AMC during the southerly wind could also relate to the smaller cloud LWP for AMC in southerly winds (Figure 1h). An AMC decoupled from the surface would limit its moisture supply and CCN supply. The limited moisture supply would reduce cloud LWP. On the other hand, it is also possible that AMCs with lower LWP would have weaker cloud top radiative cooling, hence less in-cloud turbulence, and decouple the cloud from the surface. The interaction between cloud LWP, in-cloud dynamics, and cloud lifetime warrants further investigation.

The easterly and westerly profiles in October are similar to that during a northerly wind, with RH_i greater than 100% in the cloud layer and clouds coupled to the surface (not shown). Different than in September, the easterly wind profiles in October are ~1 °C colder and ~0.3 g/kg drier than the northerly and westerly wind profiles near the surface. This is because the sea ice concentration over the Beaufort Sea usually increases from the northeast relative to the ARM NSA site, so that easterly winds bring colder and drier air over the sea ice. Similar to September, the easterly wind profiles are 2 to 5 °C warmer than the other three wind directions in the upper layers. Therefore, the RH_i profile decreases rapidly toward the cloud top during an easterly wind, which results in the lower cloud top heights for AMC during the easterly wind.

In November (Figure 4), because both the ocean and the land are covered by snow/ice, the maximum frequency of specific humidity decreases to ~1 g/kg for both wind directions, which is much drier than those in September and October. Meanwhile, the southerly wind is warmer than the northerly wind profile, especially below $Z_{b,MPL}$. Despite the drier atmosphere in November, its temperature is also relative low (<−15 °C) in the cloud layer. Both the maximum frequency and the median value of RH_i are greater than 100% in the cloud layer for both northerly and southerly winds. Moreover, the atmosphere is more stable in November than in September and October. The

stable and dry atmosphere may explain the lower AMC occurrence frequency in November.

To further investigate the relation between thermodynamics and cloud properties, the AMC occurrence frequency is calculated as a function of different thermodynamic parameters, and the regression slopes and the correlation (R-squared) of the linear relationships are shown in Table 1. The first three columns are the mean temperature, specific humidity, and RH_i at 500–600-m level, and the last column is the difference of θ_e at 500 m and at the surface. Based on the RFD of temperature for each month, the temperature range of the linear relationship is from −8 to +2, −14 to −4, and −24 to −4 ˚C for September, October, and November, respectively. The specific humidity range is from 1–6, 0–5, and 0–2.5 g/kg for September, October, and November, respectively. The range of relative humidity with respect to ice is 50% to 110%, while the θ_e difference range is −1 to 4 K for all three months.

Table 1
The Regression Slope and R-Squared Values Between Arctic Mixed-Phase Cloud Occurrence Frequency and Different Thermodynamic Variables at 500–600-m Level

Month	W_{dir}	Temperature		Specific humidity		RH_i		θ_e (500-m surface)	
		slope (%/°C)	R^2	slope %/(g/kg)	R^2	slope (%/%)	R^2	slope (%/K)	R^2
Sep	N	−1.4	0.07	**−10.7**	**0.62**	+0.3	0.06	**−4.2**	**0.40**
	S	**−7.3**	**0.84**	**−7.2**	**0.45**	**+1.2**	**0.92**	**−7.3**	**0.76**
Oct	N	**−5.3**	**0.51**	**−30.6**	**0.79**	+0.4	0.11	**−10.0**	**0.91**
	S	**−7.8**	**0.81**	−11.6	0.44	**+1.5**	**0.89**	**−8.8**	**0.69**
Nov	N	+0.5	0.10	**+21.4**	**0.57**	+0.0	0.01	−3.5	0.11
	S	+0.1	0.00	−4.2	0.06	**+0.7**	**0.45**	**−10.9**	**0.83**

Note. Results with $p < 0.05$ are marked in bold (statistical significance at 95% confidence level).

The 500–600-m level is used based on the following reasons: (1) the median $Z_{b,ceil}$ is at ~500 m for all three months (Figures 1d–1f), (2) the RH_i profile maximizes near the $Z_{b,ceil}$, and (3) larger differences in RH_i distribution are shown near the $Z_{b,ceil}$ between the northerly and southerly wind profiles. A sensitivity test using temperature, specific humidity, and RH_i values at different levels (e.g., every 100-m layer from the surface to 1,500 m) was also performed. Trends do not change with different levels, and the strongest relationship between these variables and cloud occurrence frequency is found at the 500–600-m layer.

As shown in Table 1 in September and October, AMC occurrence frequency negatively correlates to temperature for both northerly and southerly winds. The only exception is during a northerly wind in September where AMC occurrence frequency has no relationship with temperature. In November, no direct relationship is found between temperature and cloud occurrence frequency. The negative relationship between AMC occurrence frequency and temperature is possibly due to the negative correlation between temperature and relative humidity, as well as the decrease of ice growth rate with increasing temperature at a relatively warm range (e.g. −14 to +2 °C). This result is consistent with previous findings in that the possibility density function of AMC temperature peaks around −15 to −10 °C in autumn (Shupe

et al., 2006). The slopes between temperature and cloud occurrence frequency are around −5.3 to −7.8%/°C, which means that when the temperature increases by ~10 °C (Figures 2, 3a, and 3e), the AMC occurrence frequency decreases by ~53–78% with R^2 ranges from 0.51 to 0.84.

A negative relationship is found between AMC occurrence frequency and specific humidity in September and October. The negative relation between AMC occurrence frequency and temperature and specific humidity is consistent with previous results, as the mixed-phase cloud conditions are colder and drier than all low-cloud conditions in September and October (Figures 2 and 3). The slopes between specific humidity and AMC occurrence frequency are −7.2 to −30.6%/(g/kg), and the R^2 are from 0.45 to 0.79. Furthermore, this negative relationship is found for specific humidity at any level from the surface to 1,500 m, but the slopes are more negative for specific humidity at lower levels (results not shown). In November, a positive relationship exists between AMC occurrence frequency and specific humidity during the northerly wind.

When the surface wind is coming from the south, the AMC occurrence frequency increases with higher RH_i values from September to November. The slopes are ~0.7–1.5%/%, and the R^2 are ~0.9 in September and October and 0.45 in November. On the other hand, when the wind is northerly, no relationship is found between AMC occurrence frequency and RH_i values at 500–600 m or at any other levels (not shown).

As shown in the RFD profiles (Figures 2-4), atmospheric stability below $Z_{b,ceil}$ is different between northerly and southerly winds. Therefore, we investigate the relationship between AMC occurrence frequency and the difference in θ_e ($\Delta\theta_{e\ (500m\text{-}surface)}$). We also tested using the *lower tropospheric stability*, which is defined as the difference in potential temperature (θ) between the 700-hPa level and the surface, but no significant relationship was found between lower tropospheric stability and AMC properties. AMC occurrence frequency is negatively correlated with the 0–500-m stability for all three months and both wind directions, meaning that AMCs are less likely to occur when the atmosphere is more stable.

Based on the thermodynamic profiles and the relationship analysis, in October, northerly winds transport more saturated and less stable air to the ARM NSA site, which favor the formation of AMCs and explains the higher AMC occurrence frequency during the northerly wind. On the other hand, in September, no significant difference is found between northerly wind and southerly wind RH_i and stability profiles. Since the AMC occurrence frequency is negatively correlated with temperature and specific humidity in September and October, the colder and drier air mass during a southerly wind cannot explain the lower AMC occurrence frequency. An explanation for why the AMC occurrence frequency is ~20% lower during a southerly wind in September requires further investigation.

3.3 Arctic Mixed-Phase Cloud Microphysical Processes During Northerly and Southerly Winds

Similar to Figures 2-4, the radar reflectivity, spectrum width, and Doppler velocity are normalized from the cloud base to cloud top in Figure 5. Both ceilometer and MPL cloud bases are used as $Z_n = 0$ and $Z_n = -0.5$, respectively. In October, the ocean is still mostly open, while the land is increasingly covered by snow. Therefore, the comparison between the northerly and southerly winds in October should best represent the difference between marine and continental air masses and differences between open water and snow-covered surfaces. Additionally, larger differences are seen in the thermodynamics between northerly and southerly winds in October, as shown in Figures 2-4. Therefore, October AMC radar profiles are shown here to reveal different processes within the cloud and how these processes change with different air masses and surface conditions.

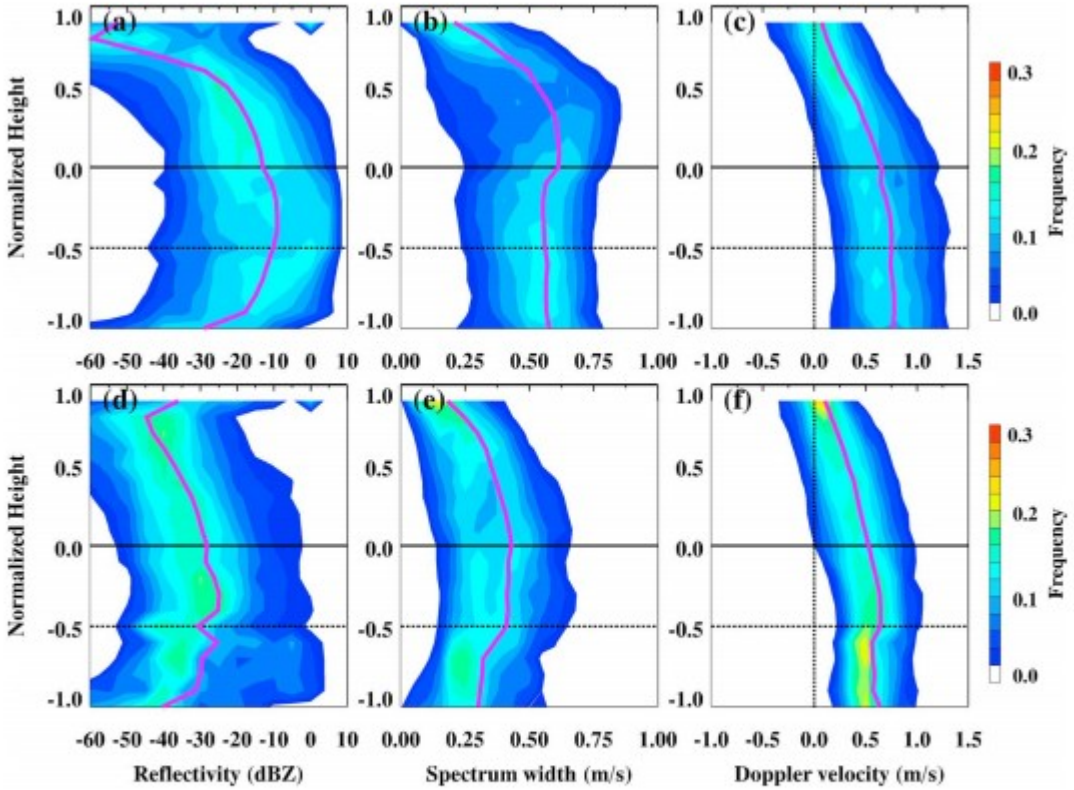

Figure 5. The relative frequency distribution contours of (a and d) radar reflectivity (dBZ), (b and e) spectrum width (m/s), and (c and f) Doppler velocity (m/s) for AMCs in October at the ARM NSA site during the period 2002–2008. The top and bottom panels represent the profiles of radar measurements during the northerly and southerly winds, respectively. Zero value for Doppler velocity is highlighted with dots in (c) and (f). Other definitions are the same as Figure 2.

At cloud top ($Z_n = 1$), the maximum frequency of radar reflectivity, spectrum width, and Doppler velocity are −50 dBZ during a northerly wind (−40 dBZ during a southerly wind), 0.25 and 0 m/s, respectively. This result is

consistent with previous findings in that at the AMC top, the hydrometers are mostly in liquid form, where AMCs have a more homogeneous distribution, and a mean fall speed close to zero (de Boer et al., 2009; Sedlar et al., 2012; Shupe et al., 2006, 2008; Sotiropoulou et al., 2014; Verlinde et al., 2007; Wang et al., 2004).

From cloud top to $Z_{b,ceil}$ (Z_n = 1 to 0), all three radar parameters increase, which means that ice particles are forming, growing, and falling out of the liquid-dominant layer. From $Z_{b,ceil}$ to $Z_{b,MPL}$ (Z_n = 0 to −0.5), which is the ice layer in the AMC (as discussed in section 2), radar reflectivity increases until the middle of this layer then decreases toward the surface (Z_n = −1). The Doppler velocity also continues to increase and maximize at the $Z_{b,MPL}$, while spectrum width is constant in this layer. Therefore, ice particles continue to grow through collision and riming processes in this layer.

From $Z_{b,MPL}$ to surface (Z_n = −0.5 to −1), all radar parameters decrease, which indicate the evaporation/sublimation of cloud particles. This evaporation/sublimation process agrees with the RH_i profile as shown in Figures 3c and 3g, as RH_i is at supersaturation or close to 100% in the cloud layer and it decreases to subsaturation below $Z_{b,MPL}$. This result also supports findings in Qiu et al. (2015), where they found that $Z_{b,MPL}$ distinguished the decrease of cloud particle number concentration. The RFDs of the lidar backscatter coefficient has also been examined (not shown). The backscatter maximizes near $Z_{b,ceil}$ with a median value ~50–80 × 10^{-6}/m·sr and sharply decreases from 20 to 30 × 10^{-6}/m·sr to 2 × 10^{-6}/m·sr below $Z_{b,MPL}$. Therefore, $Z_{b,MPL}$ should be used as the cloud boundary for the AMC, for it distinguishes different physical processes above and below, determines the atmospheric saturation level, and discriminates the decrease of cloud particle number concentration.

Furthermore, right below $Z_{b,MPL}$ during both wind directions, the RFDs of both radar reflectivity and spectrum width have higher frequencies in the larger value compared with the layer below (Figures 5a, 5b, 5d, and 5e). This increase in both signals is possibly due to the deposition of water vapor on ice particles, which may be induced by the decrease in temperature near the sub-cloud layer (Figures 3a and 3e). The deposition process would also explain the decrease in specific humidity in the sub-cloud layer, as shown in Figures 3b and 3f. The RFD of the lidar backscatter also shows higher frequency of larger backscatter coefficients in the sub-cloud layer than the layer below (not shown). Therefore, the deposition process increases both the number concentration and the size of ice crystals in the sub-cloud layer. This hypothesis needs to be evaluated by in situ measurements. The possible feedback of the deposition process in sub-cloud layer on the sedimentation, the entrainment of moisture and heat flux, and on the cloud lifetime would also need further investigations.

The peak median reflectivity during the northerly wind is ~ −10 dBZ, which is 10–15 dBZ larger than the peak in the southerly wind profile. Differences

(northerly-southerly) in spectrum width and Doppler velocity are ~ + 0.12–0.25 and +0.1–0.27 m/s, respectively. Therefore, why do the AMCs have larger particle size and stronger precipitation process during a northerly wind condition? One hypothesis is that when the wind is coming from the north and when the ocean is open, the marine air mass being transported over the ARM NSA site is less polluted and has a broader size distribution. The larger particle size would facilitate collision/accretion, more efficient riming, and secondary ice growth in the cloud layer and therefore expedite stronger precipitation (Lohmann & Feichter, 2005). During a southerly wind, the continental air is rich with CCN and IN; it would reduce the mean particle size and enhance heterogeneous ice nucleation and produces a narrower size distribution, thereby leading to less frequent precipitating events.

Figure 6 shows the joint PDF of specific humidity and radar spectrum width for northerly and southerly wind conditions. Only AMC samples are included when the radar reflectivity >−57.5 dBZ. For both wind directions during all three months, the radar spectrum width increases with specific humidity, which indicates that as the available moisture increases, the particle size distribution also broadens. Furthermore, in September and October (when the ocean is still mostly open), with a certain specific humidity, the radar spectrum width has a higher frequency in the larger spectrum width bins during northerly winds. This result is consistent with in situ measurements over the Arctic, where they found that both springtime mixed-phase clouds and summer liquid clouds had larger particle sizes and stronger precipitation process in a clean environment compared with the polluted cases (Lance et al., 2011; Maahn et al., 2017). In November (Figures 6c and 6f) as the land and ocean are both snow/ice covered, the relationships between spectrum width and specific humidity are nearly identical between northerly and southerly winds.

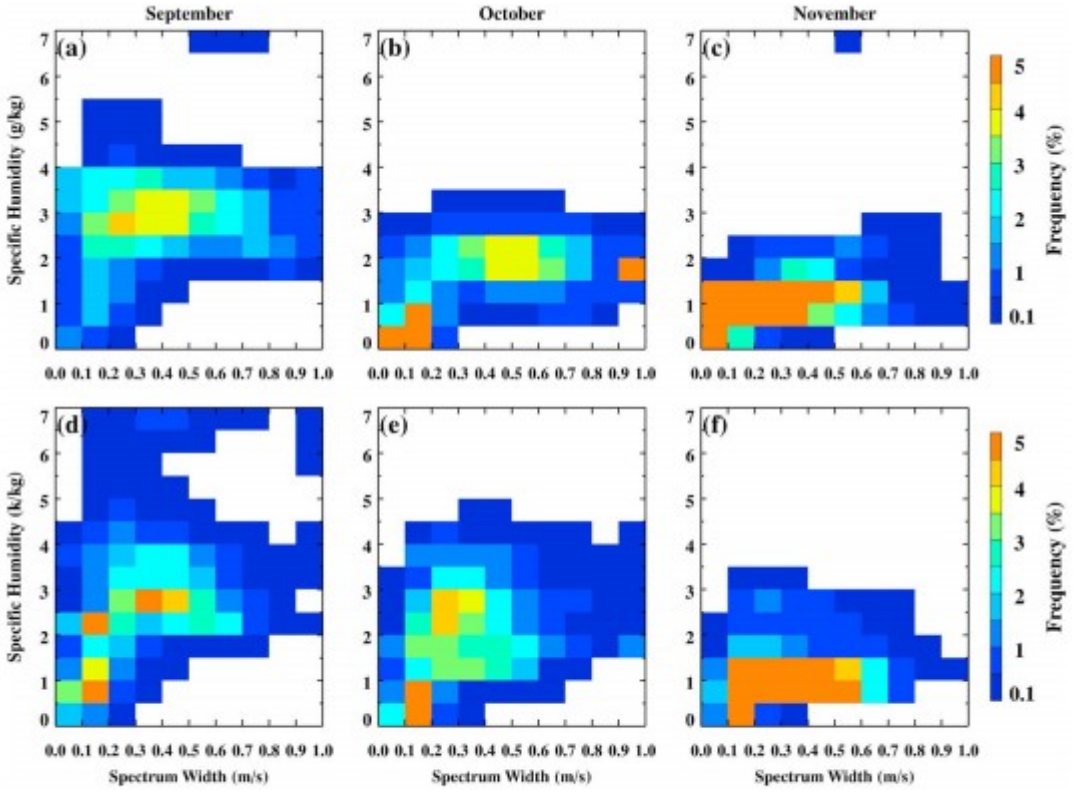

Figure 6. Joint PDFs of the radar spectrum width and specific humidity for AMCs at the ARM NSA site from September to November during the period 2002–2008. The top panel (a–c) is during the northerly wind, and the bottom panel (d–f) is during the southerly wind.

4 Summary and Discussions

To fully understand the interaction between surface condition, atmospheric properties, and cloud properties over the Arctic in the autumn season (September–November), 7 years (2002–2008) of ground-based observations at the Utqiaġvik, Atmospheric Radiation Measurement (ARM) North Slope of Alaska (NSA) site, have been analyzed. These data sets have been used to examine the frequency of occurrence of the Arctic Mixed-phase cloud (AMC), the cloud heights of AMC, the liquid water path (LWP) of AMC, the atmospheric temperature/specific humidity/RH_i/stability profiles when AMCs are present, and the radar reflectivity/spectrum width/Doppler velocity of AMCs. In addition, we investigate whether the above parameters vary with different wind direction (northerly versus southerly) and surface condition (snow free versus snow/ice). From these analyses, the following conclusions can be made:

1. The occurrence frequencies of Arctic mixed-phase cloud (AMC) are 42.1%, 49.9%, and 33.8% for September, October, and November, respectively. These values are lower than in Shupe et al. (2011) or Qiu et al. (2015), as only low-level AMCs (cloud top <3 km) are focused in this study. The ice layer thicknesses, which is defined as the difference

between ceilometer and MPL cloud base heights, are smallest in September and largest in October, and the cloud top and ceilometer base heights are highest in October and lowest in September. The mean LWPs for AMC are comparable in September (135.2 g/m^2) and October (141.5 g/m^2) and decrease to about half in November (74.8 g/m^2). From the relative frequency distribution analysis of the temperature, specific humidity, relative humidity, and potential temperature gradient profiles, the median value of the air temperature near the surface decreases from ~0 °C in September to ~ −15 °C in November. As the surface gradually becomes covered by snow and ice, the median specific humidity value decreases from ~3.5 g/kg in September to ~1.2 g/kg in November near the surface.

2. Since the Utqiaġvik site is located on the northern coast of Alaska, the atmospheric thermodynamic profiles vary with wind direction. In September and October, when the ocean is still open, the atmosphere is warmer and moister during a northerly wind (from the ocean) than during a southerly wind (from the land). Furthermore, as the sea ice concentration increases from the northeast of Utqiaġvik in October, the easterly wind is colder and drier than the westerly wind in October. The RH_i is higher and atmosphere is less stable during the northerly wind, which provide conditions favorable for AMCs to develop and sustain. In November, as the Arctic Ocean becomes covered with sea ice and snow/ice also begin to accumulate on the land, differences in moisture profiles between northerly and southerly wind become smaller and the southerly wind profiles become warmer. The AMC occurrence frequencies in September and October vary from ~30% during a southerly wind to ~40–60% for the other wind directions. In November, the variation is much smaller. We further analyze the relation between the AMC occurrence frequencies with temperature (T), specific humidity (q), RH_i, and θ_e (500-m surface). The AMC occurrence frequencies in September and October are negatively correlated with both T and q at 95% confidence level. AMC occurrence is positively correlated with q at 95% confidence in November during the northerly wind. The AMC occurrence frequencies during southerly winds for all three months are positively correlated with RH_i, while they are negatively correlated with difference in θ_e (500-m surface) at 95% confidence for all three months except for northerly winds in November.

3. The radar reflectivity, spectrum width, and Doppler velocity profiles are all relatively small at the AMC top, increase from cloud top toward cloud base, and are maximized between the ceilometer and MPL cloud bases. While below the MPL cloud base, all three radar parameters decrease toward the surface. These vertical profile signatures indicate that AMCs are dominated by liquid droplets near the cloud top and ice particles start to form and fall out from cloud top to the ceilometer

cloud base. Cloud particles continue to grow from the ceilometer cloud base to the MPL cloud base and begin to sublimate/evaporate below the MPL cloud base. Different processes in different parts of the AMC are also supported by the RH_i and lidar backscatter vertical profiles. RH_i is at supersaturation or close to 100% near the ceilometer cloud base and decreases to subsaturation below the MPL cloud base. The lidar backscatter maximizes near the ceilometer cloud base with a median value ~50–80 × 10^{-6}/m·sr and sharply decreases from 20–30 × 10^{-6}/m·sr to 2 × 10^{-6}/m·sr below the MPL cloud base. Therefore, the MPL cloud base defines the cloud boundary for the AMC, as it depicts the different physical process of cloud particles, the environment saturation level, and the decrease of cloud particle number concentration.

4. AMCs contain more ice particles and have a stronger precipitation process during the northerly wind. This is plausibly due to the marine type of air mass associated with the northerly wind being less polluted and having a broader size distribution compared with the continental type associated with the southerly wind. Therefore, larger particles with a broader size distribution would facilitate the collision/accretion process and riming and secondary ice growth. This hypothesis can be proved by the higher frequency of larger spectrum width during the northerly wind compared with the southerly wind in September and October (i.e., when the ocean is open). The *T*, *q*, and radar reflectivity, spectrum width profiles depict the deposition process in the sub-cloud layer below the MPL cloud base in September and October.

AMCs are found to have complex interactions and feedback processes with the local environment, cloud microphysics, surface conditions, aerosols, and other processes. This study provides evidence on the relationship between surface conditions, local environment, and cloud properties at a single ground site. Some questions have been raised by this study that may require further investigations. For example, why is the AMC occurrence frequency negatively correlated with specific humidity in September and October? How does AMC lifetime relate to precipitation intensity and does AMC during the northerly wind with stronger ice precipitation have longer or shorter lifetime? Future studies may also focus on the aerosol, CCN and IN properties, and the AMC microphysical properties associated with surface wind directions using either aerosol ground-based observation or in situ measurements or by simulating these cloud processes. The sub-cloud layer microphysical processes found in this study also warrant further model simulations on the water vapor feedback on AMC and cloud lifetime.

Acknowledgments

The data were obtained from the Atmospheric Radiation Measurement (ARM) Program sponsored by the U.S. Department of Energy (DOE) Office of Energy Research, Office of Health and Environmental Research, Environmental

Sciences Division. The data can be downloaded from http://www.archive.arm.gov/. The authors would like to thank Ryan Stanfield and Erica Dolinar for their contribution and suggestions on this study. We would also like to thank the Editor and three anonymous reviewers for their insightful comments and suggestions. This study was primarily supported by the NASA CERES project under grant NNX17AC52G at the University of Arizona.

References

Campbell, J. R., Hlavka, D. L., Spinhirne, J. D., Turner, D. D., & Flynn, C.J. (1998). Operational cloud boundary detection and analysis from micropulse lidar data, Proc. Eighth ARM Science Team Meeting, Tucson, AZ, U.S. Department of Energy, 119–122

Campbell, J. R., Hlavka, D. L., Welton, E. J., Flynn, C. J., Turner, D. D., Spinhirne, J. D., et al. (2002). Full-time eye-safe cloud and aerosol lidar observation at Atmospheric Radiation Measurement program sites: Instruments and data processing. *Journal of Atmospheric and Oceanic Technology*, 19(4), 431– 442. https://doi.org/10.1175/1520-0426(2002)019<0431:FTESCA>2.0.CO;2

Clothiaux, E. E., Ackerman, T. P., Mace, G. G., Moran, K. P., Marchand, R. T., Miller, M., & Martner, B. E. (2000). Objective determination of cloud heights and radar reflectivities using a combination of active remote sensors at the ARM CART sites. *Journal of Applied Meteorology*, 39(5), 645– 665. https://doi.org/10.1175/1520-0450(2000)039<0645:ODOCHA>2.0.CO;2

Clothiaux, E. E., Mace, G. G., Ackerman, T. P., Kane, T. J., Spinhirne, J. D., & Scott, V. S. (1998). An automated algorithm for detection of hydrometeor returns in micropulse lidar data. *Journal of Atmospheric and Oceanic Technology*, 15(4), 1035– 1042. https://doi.org/10.1175/1520-0426(1998)015<1035:AAAFDO>2.0.CO;2

Cohen, J., Screen, J. A., Furtado, J. C., Barlow, M., Whittleston, D., Coumou, D., et al. (2014). Recent Arctic amplification and extreme mid-latitude weather. *Nature Geoscience*, 7(9), 627– 637. https://doi.org/10.1038/ngeo2234

Curry, J. A., Rossow, W. B., Randall, D., & Schramm, J. L. (1996). Overview of arctic cloud and radiation characteristics. *Journal of Climate*, 9(8), 1731–1764. https://doi.org/10.1175/1520-0442(1996)009<1731:OOACAR>2.0.CO;2

De Boer, G., Eloranta, E., & Shupe, M. (2009). Arctic mixed-phase stratiform cloud propertiesfrom multiple years of surface-based measurements at two high-latitude locations. *Journal of the Atmospheric Sciences*, 66(9), 2874–2887. https://doi.org/10.1175/2009JAS3029.1

Devasthale, A., Sedlar, J., & Tjernström, M. (2011). Characteristics of water-vapour inversions observed over the Arctic by Atmospheric Infrared Sounder

(AIRS) and radiosondes. *Atmospheric Chemistry and Physics*, 11(18), 9813–9823. https://doi.org/10.5194/acp-11-9813-2011

Dong, X., & Mace, G. G. (2003). Arctic stratus cloud properties and radiative forcing derived from ground-based data collected at Barrow, Alaska. *Journal of Climate*, 16(3), 445– 461. https://doi.org/10.1175/1520-0442(2003)016<0445:ASCPAR>2.0.CO;2

Dong, X., Xi, B., Crosby, K., Long, C. N., Stone, R. S., & Shupe, M. D. (2010). A 10 year climatology of Arctic cloud fraction and radiative forcing at Barrow, Alaska. *Journal of Geophysical Research*, 115, D17212. https://doi.org/10.1029/2009JD013489

Flynn, C. (2004). Vaisala ceilometer (model CT25K) handbook, ARM TR-020

Holland, M. M., & Bitz, C. M. (2003). Polar amplification of climate change in coupled models. *Climate Dynamics*, 21(3–4), 221– 232. https://doi.org/10.1007/s00382-003-0332-6

Intrieri, J. M., Shupe, M. D., Uttal, T., & McCarty, B. J. (2002). An annual cycle of Arctic cloud characteristics observed by radar and lidar at SHEBA. *Journal of Geophysical Research*, 107(C10), 8030. https://doi.org/10.1029/2000JC000423

Jiang, H. J., Feingold, G., Cotton, W. R., & Duynkerke, P. G. (2001). Large-eddy simulations of entrainment of cloud condensation nuclei into the Arctic boundary layer: May 18, 1998, FIRE/SHEBA case study. *Journal of Geophysical Research*, 106(D14), 15,113– 15,122. https://doi.org/10.1029/2000JD900303

Johannessen, O. M., Bengtsson, L., Miles, M. W., Kuzmina, S. I., Semenov, V. A., Alekseev, G. V., et al. (2004). Arctic climate change: Observed and modelled temperature and sea-ice variability. *Tellus Series A*, 56(4), 328–341. https://doi.org/10.1111/j.1600-0870.2004.00060.x

Kay, J. E., Bourdages, L., Miller, N. B., Morrison, A., Yettella, V., Chepfer, H., & Eaton, B. (2016). Evaluating and improving cloud phase in the Community Atmosphere Model version 5 using spaceborne lidar observations. *Journal of Geophysical Research: Atmospheres*, 121, 4162– 4176. https://doi.org/10.1002/2015JD024699

Klein, S. A., McCoy, R. B., Morrison, H., Ackerman, A. S., Avramov, A., Boer, G., et al. (2009). Intercomparison of model simulations of mixed-phase clouds observed during the ARM mixed-phase Arctic cloud experiment. I: Single-layer cloud. *Quarterly Journal of the Royal Meteorological Society*, 135(641), 979– 1002. https://doi.org/10.1002/qj.416

Lance, S., Shupe, M. D., Feingold, G., Brock, C. A., Cozic, J., Holloway, J. S., et al. (2011). Cloud condensation nuclei as a modulator of ice processes in Arctic mixed-phase clouds. *Atmospheric Chemistry and Physics*, 11(15), 8003– 8015. https://doi.org/10.5194/acp-11-8003-2011

Liljegren, J. C., Clothiaux, E. E., Mace, G. G., Kato, S., & Dong, X. (2001). A new retrieval for cloud liquid water path using a ground-based microwave radiometer and measurements of cloud temperature. *Journal of Geophysical Research*, 106(D13), 14,485– 14,500. https://doi.org/10.1029/2000JD900817

Lin, B., Minnis, P., & Fan, A. (2003). Cloud liquid water path variations with temperature observed during the Surface Heat Budget of the Arctic Ocean (SHEBA) experiment. *Journal of Geophysical Research*, 108(D14), 4427. https://doi.org/10.1029/2002JD002851

Lohmann, U., & Feichter, J. (2005). Global indirect aerosol effects: A review. *Atmospheric Chemistry and Physics*, 5(3), 715– 737. https://doi.org/10.5194/acp-5-715-2005

Maahn, M., de Boer, G., Creamean, J. M., Feingold, G., Mc-Farquhar, G. M., Wu, W., & Mei, F. (2017). The observed influence of local anthropogenic pollution on northern Alaskan cloud properties. *Atmospheric Chemistry and Physics*, 17(23), 14,709– 14,726, https://doi.org/10.5194/acp-17-14709-2017.

Moran, K. P., Martner, B. E., Post, M. J., Kropfli, R. A., Welsh, D. C., & Widener, K. B. (1998). An unattended cloud-profiling radar for use in climate research. *Bulletin of the American Meteorological Society*, 79(3), 443– 455. https://doi.org/10.1175/1520-0477(1998)079<0443:AUCPRF>2.0.CO;2

Morris, V. R. (2012). Vaisala ceilometer (vceil) handbook, ARM TR-020.

Morrison, H., de Boer, G., Feingold, G., Harrington, J., Shupe, M. D., & Sulia, K. (2012). Resilience of persistent Arctic mixed-phase clouds. *Nature Geoscience*, 5, 11– 17.

Morrison, H., McCoy, R. B., Klein, S. A., Xie, S., Luo, Y., Avramov, A., et al. (2009). Intercomparison of model simulations of mixed-phase clouds observed during the ARM mixed-phase Arctic cloud experiment. II: Multi-layered cloud. *Quarterly Journal of the Royal Meteorological Society*, 135(641), 1003– 1019. https://doi.org/10.1002/qj.415

Najafi, M. R., Zwiers, F. W., & Gillett, N. P. (2015). Attribution of Arctic temperature change to greenhouse-gas and aerosol influences. *Nature Climate Change*, 5(3), 246– 249. https://doi.org/10.1038/nclimate2524

Nygård, T., Valkonen, T., & Vihma, T. (2013). Characteristics of Arctic low-tropospheric humidity inversions based on radio soundings. *Atmospheric Chemistry and Physics Discussions*, 13, 22,575– 22,605.

Pinto, J. O. (1998). Autumnal mixed-phase cloudy boundary layers in the Arctic. *Journal of the Atmospheric Sciences*, 55, 2,016– 2,038.

Qiu, S., Dong, X., Xi, B., & Li, J.-L. F. (2015). Characterizing Arctic mixed-phase cloud structure and its relationship with humidity and temperature inversion using ARM NSA observations. *Journal of Geophysical Research: Atmospheres*, 120, 7737– 7746. https://doi.org/10.1002/2014JD023022

Sassen, K. (1991). The polarization lidar technique for cloud research: A review and current assessment. *Bulletin of the American Meteorological Society*, 12, 1848– 1866.

Schuur, E. A. G., McGuire, A. D., Schädel, C., Grosse, G., Harden, J. W., Hayes, D. J., et al. (2015). Climate change and the permafrost carbon feedback. *Nature*, 520(7546), 171– 179.

Sedlar, J., & Shupe, M. D. (2014). Characteristic nature of vertical motions observed in Arctic mixed-phase stratocumulus. *Atmospheric Chemistry and Physics*, 14(7), 3461– 3478. https://doi.org/10.5194/acp-14-3461-2014

Sedlar, J., Shupe, M. D., & Tjernström, M. (2012). On the relationship between thermodynamic structure and cloud top, and its climate significance in the Arctic. *Journal of Climate*, 25(7), 2374– 2393. https://doi.org/10.1175/JCLI-D-11-00186.1

Sedlar, J., & Tjernström, M. (2009). Stratiform cloud-inversion characterization during the Arctic melt season. *Boundary-Layer Meteorology*, 132, 455– 474.

Serreze, M., Barrett, A., Stroeve, J., Kindig, D., & Holland, M. (2009). The emergence of surface-based Arctic amplification. *The Cryosphere*, 3, 11– 19.

Shupe, M. D. (2007). A ground-based multisensor cloud phase classifier. *Geophysical Research Letters*, 34, L22809. https://doi.org/10.1029/2007GL031008

Shupe, M. D. (2011). Clouds at Arctic atmospheric observatories. Part II: Thermodynamic phase characteristics. *Journal of Applied Meteorology and Climatology*, 50, 645– 661.

Shupe, M. D., Daniel, J. S., De Boer, G., Eloranta, E. W., Kollias, P., Long, C. N., et al. (2008). A focus on mixed-phase clouds: The status of ground-based observational methods. *Bulletin of the American Meteorological Society*, 89, 1549– 1562.

Shupe, M. D., & J. M. Intrieri (2004). Cloud radiative forcing of the Arctic surface: The influence of cloud properties, surface albedo, and solar zenith angle. *Journal of Climate*, 17, 616– 628.

Shupe, M. D., Matrosov, S. Y., & Uttal, T. (2006). Arctic mixed-phase cloud properties derived from surface-based sensors at SHEBA. *Journal of the Atmospheric Sciences*, 63, 697– 711.

Shupe, M. D., Valden, V. P., Eloranta, E., Uttal, T., Campbell, J. R., Starkweather, S. M., & Masataka, M. (2011). Clouds at Arctic atmospheric observatories. Part I: Occurrence and macro-physical properties. *Journal of Applied Meteorology and Climatology*, 50, 626– 644.

Solomon, A., Shupe, M. D., Persson, P. O. G., & Morrison, H. (2011). Moisture and dynamicalinteractions maintaining decoupled Arctic mixed-phase

stratocumulus in the presence of ahumidity inversion. *Atmospheric Chemistry and Physics*, 11, 10,127– 10,148.

Sotiropoulou, G., Sedlar, J., Tjernström, M., Shupe, M. D., Brooks, I. M., & Persson, P. O. G. (2014). The thermodynamic structure of summer Arctic stratocumulus and the dynamic coupling to the surface. *Atmospheric Chemistry and Physics Discussions*, 14, 3815– 3874. https://doi.org/10.5194/acpd-14-3815-2014

Stamnes, K., Ellingson, R. G., Curry, J. A., Walsh, J. E., & Zak, B. D. (1999). Review of science issues, deployment strategy, and status for the ARM North Slope of Alaska—Adjacent Arctic Ocean climate research site. *Journal of Climate*, 12, 46– 63.

Stokes, G. M., & Schwartz, S. E. (1994). The Atmospheric Radiation Measurement (ARM) Program: Programmatic background and design of the cloud and radiation test bed. *Bulletin of the American Meteorological Society*, 75, 1201– 1221.

Tan, I., Storelvmo, T., & Zelinka, M. D. (2016). Observational constraints on mixed-phase clouds imply higher climate sensitivity. *Science*, 352(6282), 224– 227.

Troyan, D. (2012). Merged sounding value-added product, technical report, DOE/SC-ARM/TR-087.

Turner, D. D. (1996). Comparisons of the micropulse lidar and the Belfort Laser Ceilometer at the Atmospheric Radiation Measurement Southern Great Plains Cloud and Radiation Testbed Site, paper presented at Sixth Atmospheric Radiation Measurement (ARM) Science Team Meeting, San Antonio, TX.

Verlinde, J., Harrington, J. Y., McFarquhar, G. M., Yannuzzi, V. T., Avramov, A., Greenberg, S., et al. (2007). The mixed-phase Arctic cloud experiment. *Bulletin of the American Meteorological Society*, 88, 205– 221.

Wall, C. J., Kohyama, T., & Hartmann, D. L. (2017). Low-cloud, boundary layer, and sea ice interactions over the Southern Ocean during winter. *Journal of Climate*, 30(13), 4857– 4871. https://doi.org/10.1175/JCLI-D-16-0483.1

Wang, Z., Sassen, K., Whiteman, D. N., & Demoz, B. D. (2004). Studying altocumulus with ice virga using ground-based active and passive remote sensors. *Journal of Applied Meteorology*, 43, 449– 460. https://doi.org/10.1175/1520-0450(2004)043<0449:SAWIVU>2.0.CO;2

Wesslén, C., Tjernström, M., Bromwich, D. H., de Boer, G., Ekman, A. M. L., Bai, L.-S., & Wang, S.-H. (2014). The Arctic summer atmosphere: An evaluation of reanalyses using ASCOS data. *Atmospheric Chemistry and Physics*, 14, 2605– 2624. https://doi.org/10.5194/acp-14-2605-2014

Xie, S., Liu, X., Zhao, C., & Zhang, Y. (2013). Sensitivity of CAM5-simulated Arctic clouds and radiation to ice nucleation parameterization. *Journal of Climate*, 26, 5981– 5999. https://doi.org/10.1175/JCLI-D-12-00517.1

Zuidema, P., Baker, B., Han, Y., Intrieri, J., Key, J., Lawson, P., et al. (2005). An Arctic springtime mixed-phase cloudy boundary layer observed during SHEBA. *Journal of the Atmospheric Sciences*, 62, 160– 176.